Taylor & Francis
Taylor & Francis Group

Materials Research Letters

ISSN: (Print) (Online) Journal homepage: https://www.tandfonline.com/loi/tmrl20

Metastable phase formation of $(Mo,Cr)_2AlB_2$ MAB phase thin films revealed by theory and experiments

P. J. Pöllmann, D. Bogdanovski, S. Lellig, P. Schweizer, M. Hans, C. Azina, S. Karimi Aghda, P. Zöll, D. M. Holzapfel, D. Primetzhofer, S. Kolozsvári, P. Polcik, J. Michler & J. M. Schneider

To cite this article: P. J. Pöllmann, D. Bogdanovski, S. Lellig, P. Schweizer, M. Hans, C. Azina, S. Karimi Aghda, P. Zöll, D. M. Holzapfel, D. Primetzhofer, S. Kolozsvári, P. Polcik, J. Michler & J. M. Schneider (2024) Metastable phase formation of $(Mo,Cr)_2AlB_2$ MAB phase thin films revealed by theory and experiments, Materials Research Letters, 12:1, 58-66, DOI: 10.1080/21663831.2023.2292054

To link to this article: https://doi.org/10.1080/21663831.2023.2292054

© 2023 The Author(s). Published by Informa UK Limited, trading as Taylor & Francis Group.

View supplementary material

Published online: 13 Dec 2023.

Submit your article to this journal

Article views: 374

View related articles

View Crossmark data

Full Terms & Conditions of access and use can be found at
https://www.tandfonline.com/action/journalInformation?journalCode=tmrl20

MATER. RES. LETT.
2024, VOL. 12, NO. 1, 58–66
https://doi.org/10.1080/21663831.2023.2292054

MATERIALS RESEARCH LETTERS
Taylor & Francis
Taylor & Francis Group

ORIGINAL REPORTS

OPEN ACCESS Check for updates

Metastable phase formation of $(Mo,Cr)_2AlB_2$ MAB phase thin films revealed by theory and experiments

P. J. Pöllmann[a], D. Bogdanovski[a], S. Lellig[a,b], P. Schweizer[b], M. Hans[a], C. Azina[a], S. Karimi Aghda[a], P. Zöll[a], D. M. Holzapfel [a], D. Primetzhofer[c], S. Kolozsvári[d], P. Polcik[d], J. Michler[b] and J. M. Schneider[a,e]

[a]Materials Chemistry, RWTH Aachen University, Aachen, Germany; [b] Empa, Swiss Federal Laboratories for Materials Science and Technology, Laboratory for Mechanics of Materials and Nanostructures, Thun, Switzerland; [c]Department of Physics and Astronomy, Uppsala University, Uppsala, Sweden; [d] Plansee Composite Materials GmbH, Lechbruck am See, Germany; [e] Max-Planck-Institut für Eisenforschung GmbH, Department Structure and Nano-/ Micromechanics of Materials, Group Self-Reporting Materials, Düsseldorf, Germany

ABSTRACT

A $(Mo_{0.24}Cr_{0.76})_{0.40}Al_{0.32}B_{0.28}$ thin film was deposited by direct current magnetron sputtering at 600 °C substrate temperature. Analysis by X-ray diffraction, energy-dispersive X-ray spectroscopy, elastic recoil detection analysis, and high-resolution scanning transmission electron microscopy revealed the formation of the previously unreported $(Mo,Cr)_2AlB_2$ MAB phase, along with Cr_3AlB_4, CrB_4, and Mo, in good agreement with density functional theory (DFT) calculations. Hence, the MAB phase family in the Mo-Cr-Al-B system is extended by a novel, quaternary member.

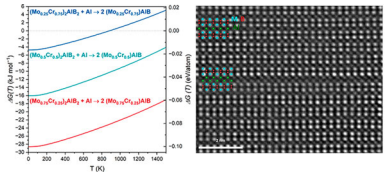

ARTICLE HISTORY
Received 13 September 2023

KEYWORDS
MAB phase; density functional theory; magnetron sputtering; phase formation; thin film

IMPACT STATEMENT

In this work, quaternary MAB phase $(Mo,Cr)_2AlB_2$ is synthesized experimentally for the first time. Its metastable formation is rationalized by density functional theory calculations.

Introduction

For many years, layered transition metal carbides/nitrides, the so-called MAX phases, where M designates an early transition metal, A is an A-group element, and X is either carbon or nitrogen, have received substantial scientific attention and were thoroughly studied due to their desirable combination of ceramic properties like high stiffness [1,2] along with metallic properties like good machinability [3], resulting from their nanolaminated structure of M-X structural unit layers interleaved by A layers and thus exhibiting a combination of covalent/ionic as well as metallic bonds [3]. Furthermore, MAX phases have shown to be high-temperature oxidation-resistant [4] as well as self-healing [5,6] and self-reporting [7].

Recently, their structurally similar cousins, the MAB phases, where B represents boron, have drawn the research community's interest, partly due to their promising and potentially application-relevant properties. Examples of such properties are the magnetocaloric effect for Fe_2AlB_2 [8], with envisioned future use in environmentally friendly cooling applications [9], low toxicity for Cr_2AlB_2 [10], of potential interest for novel forms of drug delivery in medicine, as well as good mechanical properties for a variety of compounds qualifying them for applications in aerospace and high-temperature structural components [11–13]. The first-ever reported [14] and most-studied MAB phase, MoAlB, exhibits low electrical resistivity (< 0.68 μΩm) [11,15], high thermal stability up to 1434 °C in vacuum and Ar

CONTACT P. J. Pöllmann poellmann@mch.rwth-aachen.de Materials Chemistry, RWTH Aachen University, Kopernikusstr. 10, 52062 Aachen, Germany

Supplemental data for this article can be accessed online at https://doi.org/10.1080/21663831.2023.2292054.

© 2023 The Author(s). Published by Informa UK Limited, trading as Taylor & Francis Group.
This is an Open Access article distributed under the terms of the Creative Commons Attribution License (http://creativecommons.org/licenses/by/4.0/), which permits unrestricted use, distribution, and reproduction in any medium, provided the original work is properly cited. The terms on which this article has been published allow the posting of the Accepted Manuscript in a repository by the author(s) or with their consent.

atmosphere [11], self-healing behavior [16], and excellent high-temperature oxidation resistance up to 1600 °C [17,18], rendering it a promising candidate for various applications. Furthermore, it was demonstrated that MoAlB can be synthesized in thin film form, exhibiting behavior comparable to that of the bulk material [19,20]. As early as 1995, the family of MAB phases was expanded towards quaternary $(Mo_{1-x}Cr_x)AlB$ compounds, with the reported successful synthesis of bulk $(Mo_{0.61}Cr_{0.39})AlB$ single crystals [21]. In a follow-up investigation, the homogeneity range was proposed to be $0 \leq x \leq 0.4$, and the properties of the studied Mo-rich compositions were compared to those of MoAlB. While the oxidation resistance in air was found to be comparable, the hardness increased upon Cr addition, concurrent with a decrease in the electrical resistivity [15].

In contrast to MoAlB, the formation of the equistoichiometric CrAlB phase has not been reported experimentally so far, however, the MAB phases Cr_2AlB_2, Cr_3AlB_4, and Cr_4AlB_6 have all been synthesized [22–25]. Enthalpies of formation (ΔH) and Gibbs reaction energies (ΔG), both determined at 0 K, indicate that $Cr_2AlB_2 + Al$ is more stable than CrAlB ($Cr_2Al_2B_2$, also referred to as 222 type) [26–29]. However, for accurate phase formation predictions, considering the temperature dependence of the Gibbs energy ($\Delta G(T)$) is vital. Therefore, expanding on the previously mentioned reports, in our recent study we investigated the temperature-dependent energetic barriers towards CrAlB and (Mo,Cr)AlB formation using density-functional theory (DFT) calculations [30]. While the CrAlB phase was metastable in terms of formation energy, when compared to its energetically most preferred competing phase, Cr_2AlB_2, which may explain the lack of experimental reports on this phase, the calculated energetic difference of ≈ 0.008 eV/atom (≈ 10 kJ mol^{-1}) is very small and may well be overcome in kinetically limited synthesis processes such as physical vapor deposition (PVD). Moreover, alloying with Mo has been found to cause changes in chemical bonding, leading to increased stability of $(Mo_{1-x}Cr_x)AlB$: Comparing the quaternary phase to competing ternaries Mo_2AlB_2 and Cr_2AlB_2 as well as Al at 0 K, formation of the 222 solid solution phase is enabled at $x \lessapprox 0.67$ [30]. Furthermore, even at finite temperatures, the temperature-dependent Gibbs energies of formation also show a decreasing trend with increasing Mo content, causing $(Mo_{0.375}Cr_{0.625})AlB$ to be stable, when compared to Mo_2AlB_2 at temperatures of up to approx. 650 K, indicating possible formation, with further energetic stabilization at higher temperatures for higher Mo contents [30].

Thus far, however, experimental studies in the Mo–Cr-Al-B system were limited to high Mo contents, whereas the Cr-rich compositions remain unexplored. Furthermore, existing studies pertain to bulk synthesis methods, where high temperatures and long holding times are required. As higher Cr contents are expected to improve the corrosion resistance [31] while simultaneously reducing electrical resistivity [15] we probe this previously unexplored composition window regarding the phase formation during direct current magnetron sputtering. We report the formation of the novel MAB phase compound $(Mo,Cr)_2AlB_2$ along with several minority phases and rationalize their formation in terms of energetics based on DFT calculations.

Materials and methods

Experimental details

The MoCrAlB thin film was synthesized by magnetron sputtering in a high vacuum deposition system with a base pressure of $< 9 \times 10^{-7}$ mbar at room temperature, and $< 5 \times 10^{-6}$ mbar at the deposition temperature of 600°C. This temperature was selected since prior results in related material system MoAlB revealed the highest density [20]. A substrate-facing 2" Cr-Al-B 1:1:1 composite target (Plansee Composite Materials GmbH, Lechbruck am See, Germany) was run in direct current (DC) mode at a constant power of 120 W, whereas for an elemental 2" molybdenum target (FHR Anlagenbau GmbH, Ottendorf-Okrilla, Germany), mounted at a 45° angle to the substrate normal, the DC power was set to 10 W (Figure 1). The target-to-substrate distance for both targets was 10 cm and a one-side polished 10×10 mm-sized Al_2O_3 (0001) single-crystalline substrate was kept at a floating potential during deposition. To enhance heat absorption and dissipation of the radiation supplied by the halogen lamp heater as well as to maintain a uniform substrate temperature, the unpolished substrate side was coated with a thin layer of TiN before the deposition. An Ar pressure of 0.3 Pa and a deposition time of 1 h yielded a MoCrAlB thin film with a thickness of about 1.1 µm.

Time-of-flight elastic recoil detection analysis (ToF-ERDA) was carried out at the Tandem Accelerator Laboratory of Uppsala University [32] using a 36 MeV $^{127}I^{8+}$ primary beam. The incidence and exit angle of the primary ions and detected recoils with respect to the film surface was 22.5°, while the angle between the primary beam and the detector telescope was 45°. The time-of-flight was measured with thin carbon foils [33] and a gas detector system was employed for energy discrimination [34]. A depth profile was created from time-energy coincidence spectra using CONTES [35]. The average concentration was extracted from this profile, excluding the oxygen-rich near-surface region. A maximum total

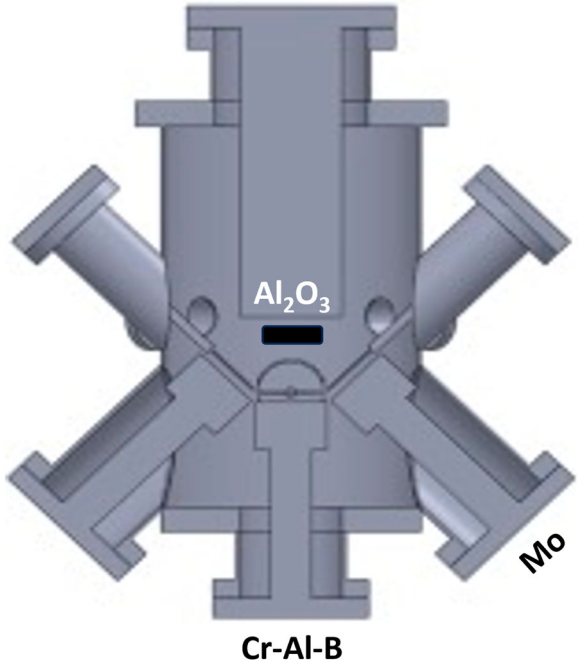

Figure 1. Schematic illustration of the deposition setup used here comprising of a substrate-facing Cr-Al-B and a 45°-angled Mo target.

uncertainty of 5% of the deduced values is assumed for B and aliquot fractions thereof for the metals Mo, Cr, and Al.

To study phase formation, Bragg–Brentano X-ray diffraction (XRD) was carried out in a Panalytical Empyrean MRD diffractometer (Malvern Panalytical, Almelo, The Netherlands) equipped with a Cu Kα source. The $-5°$ omega offset scans were performed with a step size of 0.026° and a measurement time of 100 s/step, while the diffractometer was operated at a current of 40 mA and a voltage of 40 kV.

A thin lamella for high-resolution scanning transmission electron microscopy (HRSTEM) investigations was prepared by focused ion beam (FIB) techniques in a Helios 5 Hydra UX dual-beam microscope (Thermo Fisher Scientific, Waltham, USA). First, a $10 \times 2.5 \times 0.1$ µm carbon layer was applied using the electron beam with 2 kV and 23 nA to protect the surface from interaction with the ion beam. Subsequently, the thickness of the carbon protection layer was increased to 1 µm using an Xe^+ plasma at 12 kV and 0.1 nA. Trenches were milled at a voltage and current of 30 kV and 60 nA, respectively, followed by lift-out and attachment of the lamella to an omniprobe lift-out grid. After thinning the lamella to approx. 500 nm, a 200 nm thick carbon protection layer was applied to both sides of the lamella at 0.1 nA to fill porous regions of the film material. Final thinning to < 100 nm lamella thickness was done with Ga^+ ions at 30 kV in an FEI Helios Nanolab 600 dual-beam microscope (Thermo Fisher Scientific, Waltham, USA) as well as in a Lyra FIB/SEM dual-beam system (Tescan, Brno, Czech Republic) with a final polishing at 5 kV. The lamella was subsequently analyzed by HRSTEM using a Titan Themis 200 G3 equipped with a SuperX EDX detector (Thermo Fisher Scientific, Waltham, USA) at an acceleration voltage of 200 kV. The corrector was tuned to 27 mrad to perform HRSTEM (dwell time: 100 ns, current: 200 pA, spotsize: 5, aperture: 50). For the EDX measurements, a dwell time of 4 µs was chosen and for the quantification, the well-established Cliff-Lorimer method was used to compare the atomic ratios of different elements within one measurement (EDX map). A beam spread of 1.75 Å was calculated with the theory developed by Goldstein et al. and Jones [36] resulting in a spatial resolution of 2.4 Å after Michael et al. [37] for a beam size of approximately 200 pm [36].

Computational details

Temperature-dependent Gibbs energies of formation were calculated using a lattice dynamics approach based on DFT calculations. The Vienna ab initio Simulation Package (VASP, version 5.4.4, University of Vienna) was employed for the DFT runs [38–40]. The projector-augmented wave method [41,42] was used to generate the basis set, using a plane-wave cutoff energy of 500 eV, while the well-established generalized gradient approximation (GGA) functional as parametrized by Perdew, Burke, and Ernzerhof (PBE) [43] was used to treat electronic exchange and correlation. The valence electron configurations modeled by the employed atomic potentials were $5s^2 4d^4 4s^2 4p^6$ for Mo, $4s^2 3d^4 3p^6$ for Cr (incorporating semi-core states for both transition metal species), $3s^2 3p^1$ for Al, and $2s^2 2p^1$ for B. The k mesh in the irreducible Brillouin zone was constructed using the Monkhorst–Pack method [44], with a density chosen to ensure energetic convergence up to 10^{-3} eV for each system and verified *via* convergence tests; as the k mesh dimensions varied for each system, they will not be listed in full. Finally, the Methfessel-Paxton method [45] of order 1 was chosen for Brillouin zone integration.

Initial structural data for all MAB phases were taken from literature [22] and the structural models were subsequently fully optimized in the ground state. The quaternary compositions were generated by successively replacing Cr with Mo to model the compositions $(Mo_{1-x}Cr_x)AlB$, $(Mo_{1-x}Cr_x)_2AlB_2$, and $(Mo_{1-x}Cr_x)_3AlB_4$ with $x = 0.25$, 0.5, and 0.75 resulting in multiple distinct ordered configurations for each composition. These configurations were subsequently fully optimized and the configuration obtaining the lowest total energy was selected for further investigation. These

optimized models served as input for the lattice dynamics runs using VASP and the *phonopy* package (version 2.11.0, University of Kyoto) [46] as the postprocessing code. Depending on the symmetry of the system, a varying number of nearly-cubic supercells were automatically generated using *phonopy*, by replacing symmetry-inequivalent atoms from their equilibrium positions. The lattice parameters *a, b, c* of these supercells were always constrained to > 10 Å preventing interactions of the displaced atoms with their periodic images. This approach is described in greater detail in prior literature [47] and our preceding publication [30].

After obtaining the *G(T)* datasets for all MAB phases and competing phases, the Gibbs energies of formation were calculated using the formula.

$$\Delta G(T) = \Sigma x G(T)(\text{product}) - \Sigma\, y\, G(T)(\text{starting materials}),$$

with x and y signifying the stoichiometric coefficients of the individual compounds/elements.

Results and discussion

Figure 2 shows the XRD pattern of the synthesized sample with the ERDA-determined average composition obtained from the depth profile (Supplementary Figure S1) of $(Mo_{0.24}Cr_{0.76})_{0.40}Al_{0.32}B_{0.28}$. The sample is identified as a phase mixture of $(Mo_{0.25}Cr_{0.75})_2AlB_2$ (simulated interplanar distances obtained from DFT calculations at 0 K) and Cr_3AlB_4 (01-084-8900) MAB phases as well as CrB_4 (01-084-8449) and Mo (00-042-1120) as additional phases with $(Mo_{0.25}Cr_{0.75})_2AlB_2$ being the predominant phase. Formation of this novel MAB phase is indicated by the peaks corresponding to the (020), (110), (021), (130), (111), (060), (061), and (151) planes which are unique to $(Mo_{0.25}Cr_{0.75})_2AlB_2$. It can be readily seen that peaks of $(Mo_{0.25}Cr_{0.75})_2AlB_2$, when compared to the ternary MAB phase Cr_2AlB_2 (01-084-8899, comparison of d spacing and 2θ values shown in Supplementary Table S2), exhibit a shift towards lower angles. This is most likely caused by the substitution of Cr atoms by the larger Mo atoms ($\approx$10% larger metallic radius compared to Cr [48]) and the resulting increase in lattice spacing. Both Cr_3AlB_4 and CrB_4 peaks also exhibit a slight shift towards lower angles, which may indicate that small quantities of Mo are also dissolved in their respective Cr host lattices.

Our prior DFT calculations suggest the quaternary $(Mo_{1-x}Cr_x)AlB$ MAB phase (further referred to as 222, signifying the (Mo,Cr):Al:B ratio, with the same nomenclature for all phases shown for enhanced clarity in Figure 3) to be stabilized in the ground state at $x \lessapprox 0.67$ [30], however, the quaternary 212 or 314 configurations have not been studied before.

Therefore, in Figure 4, calculations of the Gibbs energy of formation in the temperature range between 0 and 1500 K are shown for various MAB phase formation reactions in the Mo-Cr-Al-B system. Figure 4(a) shows the formation of the (Mo,Cr)AlB solid solution MAB phase from MoAlB and Cr_2AlB_2. The quaternary (Mo,Cr)AlB phase is metastable throughout the whole studied temperature range when compared to the two ternary MAB phases. However, the energetic barriers for its formation are rather small (max. 0.062 eV/atom for $(Mo_{0.25}Cr_{0.75})AlB$ at 1500 K) and may be readily overcome in metastable synthesis scenarios such as PVD. It has been shown that other metastable material systems like (Ti,Al)N, (V,Al)N, and $Mo_3Al_2B_4$ that can be synthesized by utilization of a PVD process [50–52]. For example, the energy of formation in the ground state for $Ti_{0.5}Al_{0.5}N$ is predicted to be $\approx$0.123 eV/atom [53] and is therefore about half an order of magnitude higher than the max. value for $(Mo_{0.25}Cr_{0.75})AlB$. Furthermore, one can observe a trend of increased stability with increasing Mo content for the 222 solid solution phase, which is in excellent agreement with both our previous *ab initio* predictions (for this quaternary 222 phase) [30] and prior experimental reports of this phase at compositions between $0 \leq x \leq 0.4$ for $(Mo_{1-x}Cr_x)AlB$ [15,21]. In Figure 4(b), where the formation of the quaternary 222 phase out of the $(Mo,Cr)_2AlB_2$ phase and elemental Al is shown, a similar picture arises: with increasing Mo content, the (Mo,Cr)AlB phase is becoming more stable and concomitantly the stability of the 212-$(Mo,Cr)_2AlB_2$ phase decreases in relation. Moreover, the formation of the 222 phase is energetically favoured for all studied compositions except for that with the lowest Mo content, where, after a crossover point at approximately 900 K ($\approx$627 °C), the formation of the 212 phase is more favorable. This is in very good agreement with the synthesis temperature of 600 °C used for the presented sample. The difference between equilibrium calculations and experiments may originate from the deviation from thermodynamic equilibrium during plasma processing.

Comparing the Gibbs energies of the formation of quaternary $(Mo,Cr)_2AlB_2$ from the ternaries MoAlB and Cr_2AlB_2 in Figure 4(c), similar to the results for the quaternary 222 phase (Figure 4(a)), the two ternary MAB phases are energetically favoured throughout the studied temperature range. At max. 0.079 eV/atom in the ground state, the energetic barrier towards the quaternary phase formation is slightly larger but may still be overcome in a metastable synthesis scenario, as outlined before. However, for the 212 phase, the stability trend with respect to the Mo content is reversed: the lower

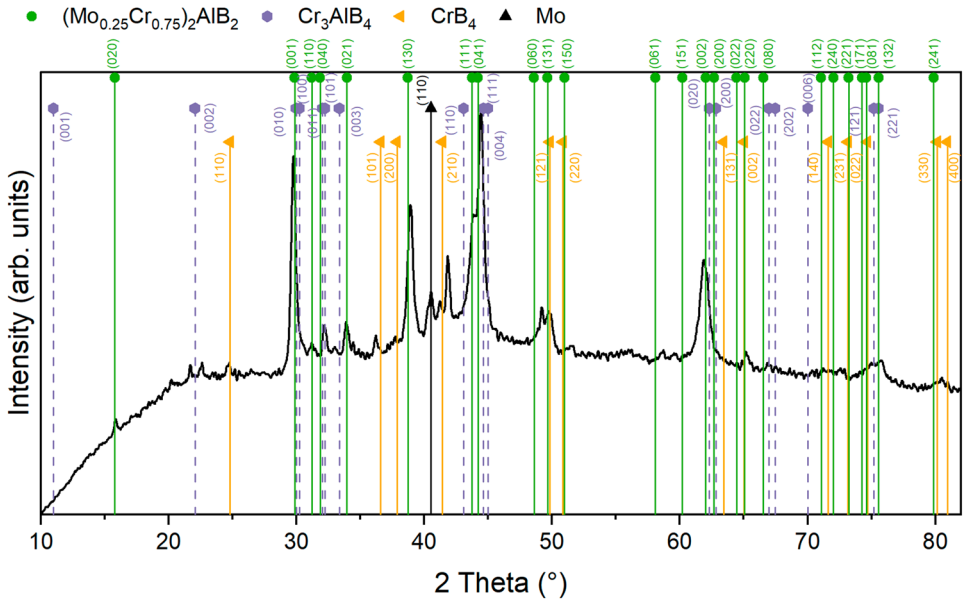

Figure 2. X-ray diffractogram from a −5° omega offset scan.

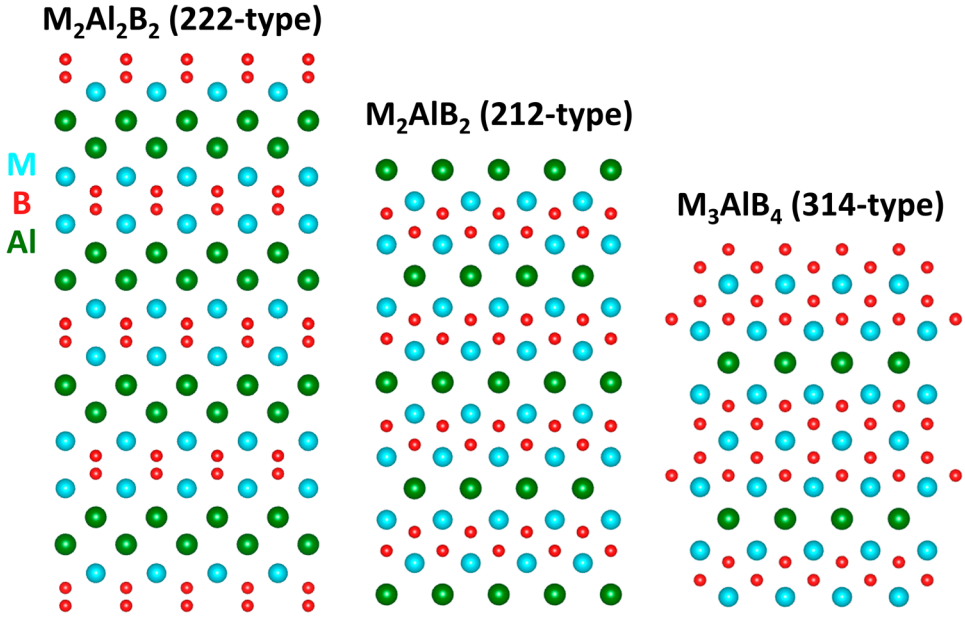

Figure 3. Ideal MAB phase structures used for DFT calculations. M designates either molybdenum or chromium, Al aluminum, and B boron [49].

the Mo content, the more stable the quaternary composition becomes in relative terms, as also observed in Figure 4(b). This is in good agreement with the XRD results above, where the $(Mo_{0.25}Cr_{0.75})_2AlB_2$ phase was identified, while the simulated diffraction patterns for higher Mo contents did not fit the measured diffractogram. Finally, Figure 4(d) depicts the formation of the quaternary $(Mo,Cr)_3AlB_4$ phase from $(Mo,Cr)_2AlB_2$ and ternary Cr_3AlB_4. It is evident, that the 314 quaternary phase is unstable throughout the whole investigated temperature range for all Mo/Cr ratios, with the magnitude of the energetic barrier being above 125 kJ mol^{-1} $\approx$0.166 eV/atom for all compositions and temperatures and thus likely too high to be overcome, even in a kinetically limited synthesis scenario. Furthermore, the most stable quaternary 212 composition is once more the Cr-rich $(Mo_{0.25}Cr_{0.75})_2AlB_2$, as observed before (Figure 4(b,c)). These results are again in excellent agreement with the X-ray diffraction data in Figure 2, identifying a phase mixture of $(Mo_{0.25}Cr_{0.75})_2AlB_2$ as well as Cr_3AlB_4 along with impurity phases.

These observations notwithstanding, in Figure 5(a), representative HRSTEM images accompanied by the corresponding EDX line scan (Figure 5(c)), recorded in the

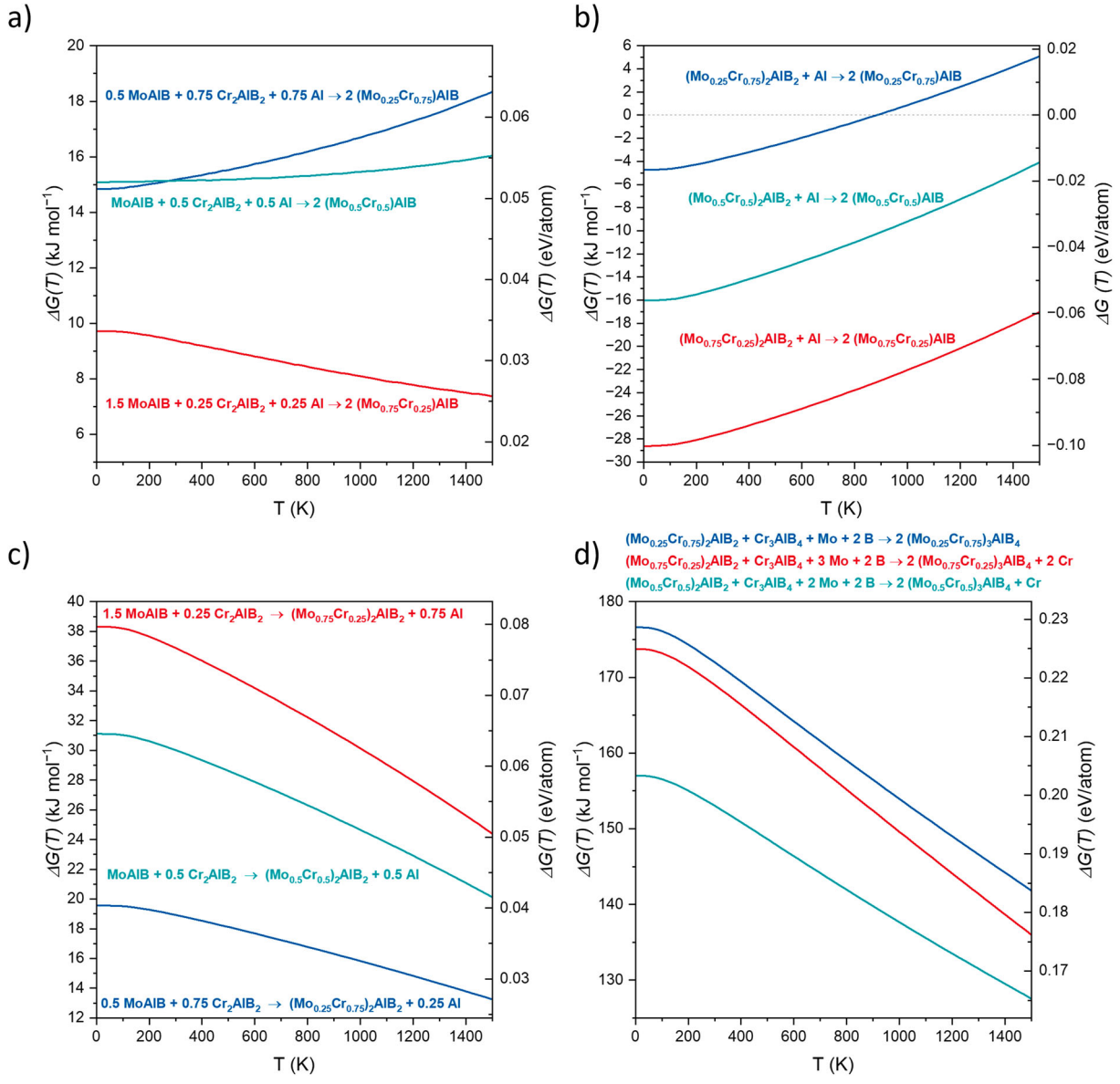

Figure 4. Temperature-dependent Gibbs energies of formation (ΔG(T)) of 222-(Mo,Cr)AlB from MoAlB and Cr_2AlB_2 (a); 222-(Mo,Cr)AlB from 212-$(Mo,Cr)_2AlB_2$ (b), $(MoCr)_2AlB_2$ from MoAlB and Cr_2AlB_2 (c), and 314-$(Mo,Cr)_3AlB_4$ from 212-$(Mo,Cr)_2AlB_2$ and Cr_3AlB_4 (d).

area specified by the orange box (Figure 5(b)) are shown, along with an overlay of ideal structural models for easier distinction of the present phases, where blue atoms correspond to Mo/Cr (= M), green atoms to Al, and red atoms to B (see Figure 3) [49]. It can be seen that, in line with the XRD results, the nanolaminated $(Mo,Cr)_2AlB_2$ MAB phase is prominent, with double MB layers separated by single Al layers. In the corresponding EDX line scan, the Al, Cr, and Mo concentration modulations mirror the nanolaminated structure of this phase, which is clearly visible in the HRSTEM image (Figure 5(a)). Moreover, the Mo/Cr ratio of the averaged concentrations along the line scan computes to 0.35 and hence is in good agreement with the $(Mo_{0.25}Cr_{0.75})_2AlB_2$ composition identified by ERDA and XRD (Figure 2) and predicted to be the most stable $(Mo,Cr)_2AlB_2$ composition by DFT calculations (Figure 4(b,c)). The slightly higher Mo/Cr ratio might result from measurement inaccuracies inherent in EDX or the very localized nature of the TEM analysis.

Furthermore, a double Al layer can be seen in Figure 5(a,b) as well as in multiple regions in Supplementary Figure S3, indicating the local formation of a compositional defect with a 222-like Al stacking. Such so-called intergrown structures were previously observed for MAX [54,55] and MAB [52] phases, where different stacking orders were reported. This is also in line with the integral structural analysis since the minute compositional defect with a 222-like Al stacking identified by HRSTEM cannot be detected by XRD. While the Gibbs energy of

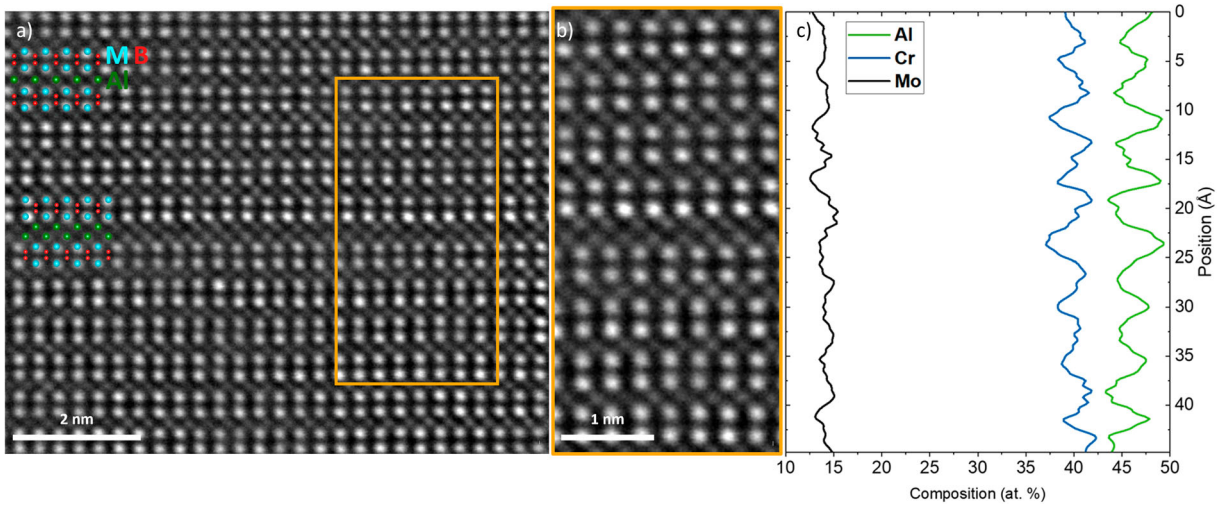

Figure 5. HAADF HRSTEM micrograph along with the corresponding EDX line scan (b–c). Atoms in representative overlay (a) correspond to Mo/Cr (blue), Al (green), and B (red) [49].

formation data indicate that 222-(Mo,Cr)AlB MAB phase is not stable throughout the investigated temperature range of 0–1500 K, when compared to the ternary MAB phases MoAlB and Cr_2AlB_2 (Figure 4(a)), the energetic barrier of $\leq$ 0.063 eV/atom may well be overcome in the here-applied PVD process. Hence, correlating the predicted formation energies for the Cr-rich 222 and 212 compositions (Figure 4(a–c)) and considering the energetic barrier, the observed concurrent formation of 212 phase and 222-like compositional defect has to be expected for the employed synthesis technique.

Conclusions

A quaternary $(Mo_{0.24}Cr_{0.76})_{0.40}Al_{0.32}B_{0.28}$ thin film was synthesized by direct current magnetron sputtering at 600 °C by co-sputtering a compound CrAlB and an elemental Mo target. Phase and composition analysis by XRD, EDX, ERDA, and HRSTEM revealed the formation of the hitherto unreported MAB phase $(Mo,Cr)_2AlB_2$, extending the family of potentially application-relevant MAB phases, along with the competing MAB phase Cr_3AlB_4 as well as CrB_4 and Mo. Furthermore, the formation of the novel quaternary 212-MAB phase was rationalized by temperature-dependent Gibbs energy of formation calculations obtained by DFT, showing that, the energetic barriers towards phase formation are small enough to be overcome in a kinetically limited synthesis scenario, while the formation of the 314-$(Mo,Cr)_3AlB_4$ phase is energetically disfavoured versus the here observed Cr_3AlB_4 phase.

Acknowledgements

D. B. and J. M. S. thank the IT Center of RWTH Aachen University for the provision of computational resources and IT support via the Jülich-Aachen Research Alliance's (JARA) JARA0221 grant and acknowledge the financial support of the NHR4CES consortium within the framework of the Materials Design SDL. J. M. S. acknowledges financial support from the MPG fellow program. Transnational access to ion beam analysis has been supported by the RADIATE project under Grant Agreement 824096 from the EU Research and Innovation programme HORIZON 2020. Accelerator operation at Uppsala University has been supported by the Swedish research council VR-RFI under grant agreement #2019-00191.

Disclosure statement

No potential conflict of interest was reported by the authors.

Funding

This work was supported by Horizon 2020 Framework Programme: [Grant Number 824096]; Max-Planck-Gesellschaft: [Grant Number Fellow program]; IT Center of RWTH Aachen University via Jülich-Aachen Research Alliance (JARA): [Grant Number JARA0221]; NHR4CES; Swedish Research Council VR RFI: [Grant Number #2019-00191].

Author contributions

P.J.P.: Conceptualization, methodology, formal analysis, investigation (lead), data curation, writing—original draft, and visualization. D.B.: Conceptualization, methodology, formal analysis, investigation, and writing—review and editing. S.L.: Investigation, formal analysis, and writing—review and editing. M.H.: Investigation, formal analysis, data curation, and writing—review and editing. C.A.: Investigation, formal analysis, and writing – review and editing. P.S.: Investigation, formal analysis, and writing—review and editing. D.M.H.: Investigation and writing—review and editing. P.Z.: Investigation and writing—review and editing. S.K.A.: Conceptualization

and writing—review and editing. D.P.: Investigation, formal analysis, writing—review and editing, and funding acquisition. S.K.: Resources and writing—review and editing. P.P.: Resources and writing—review andediting. J.M.: Funding acquisition and writing—review and editing. J.M.S.: Conceptualization, methodology, project administration, writing—original draft, supervision, and funding acquisition.

Conflicts of interest

There are no conflicts to declare.

ORCID

D. M. Holzapfel http://orcid.org/0000-0002-0374-094X

References

[1] Hettinger JD, Lofland SE, Finkel P, et al. Electrical transport, thermal transport, and elastic properties of M2AlC (M = Ti, Cr, Nb, and V). Phys Rev B. 2005 Sep;72(11):6.

[2] Schneider JM, Sigumonrong DP, Music D, et al. Elastic properties of Cr2AlC thin films probed by nanoindentation and ab initio molecular dynamics. Scr Mater. 2007;57(12):1137–1140. doi:10.1016/j.scriptamat.2007.08.006

[3] Barsoum MW. The MN+1AXN phases: A new class of solids; thermodynamically stable nanolaminates. Prog Solid State Chem. 2000;28(1-4):201–281. doi:10.1016/S0079-6786(00)00006-6

[4] Hajas DE, Baben MT, Hallstedt B, et al. Oxidation of Cr2AlC coatings in the temperature range of 1230 to 1410°C. Surf Coat Technol. 2011;206(4):591–598. doi:10.1016/j.surfcoat.2011.03.086

[5] Farle A, Boatemaa L, Shen L, et al. Demonstrating the self-healing behaviour of some selected ceramics under combustion chamber conditions. Smart Mater Struct. 2016;25(8):084019, doi:10.1088/0964-1726/25/8/084019

[6] Li SB, Xiao LO, Song GM, et al. Oxidation and crack healing behavior of a fine-grained Cr_2AlC ceramic. J Am Ceram Soc. 2013;96(3):892–899. doi:10.1111/jace.12170

[7] Stelzer B, Chen X, Bliem P, et al. Remote tracking of phase changes in Cr_2AlC thin films by in-situ resistivity measurements. Sci Rep. 2019;9:7, doi:10.1038/s41598-019-44692-4

[8] Tan X, Chai P, Thompson CM, et al. Magnetocaloric effect in $AlFe_2B_2$: toward magnetic refrigerants from earth-abundant elements. J Am Chem Soc. 2013;135(25):9553–9557. doi:10.1021/ja404107p

[9] Franco V, Blázquez JS, Ingale B, et al. The magnetocaloric effect and magnetic refrigeration near room temperature: materials and models. Annu Rev Mater Res. 2012;42(1):305–342. doi:10.1146/annurev-matsci-062910-100356

[10] Rosli NF, Nasir MZM, Antonatos N, et al. Max and MAB phases: two-dimensional layered carbide and boride nanomaterials for electrochemical applications. ACS Applied Nano Materials. 2019;2(9):6010–6021. doi:10.1021/acsanm.9b01526

[11] Kota S, Sokol M, Barsoum MW. A progress report on the MAB phases: atomically laminated, ternary transition metal borides. Int Mater Rev. 2020;65(4):226–255. doi:10.1080/09506608.2019.1637090

[12] Zhou Y, Xiang H, Dai F-Z, et al. Electrical conductive and damage-tolerant nanolaminated MAB phases Cr_2AlB_2, Cr_3AlB_4 and Cr_4AlB_6. Mater Res Lett. 2017;5(6):440–448. doi:10.1080/21663831.2017.1317047

[13] Zhang H, Dai F-Z, Xiang H, et al. Phase pure and well crystalline Cr_2AlB_2: a key precursor for two-dimensional CrB. J Mater Sci Technol. 2019;35(8):1593–1600. doi:10.1016/j.jmst.2019.03.031

[14] Halla F, Thury W. Über boride von molybdän und wolfram. Zeitschrift für Anorganische und Allgemeine Chemie. 1942;249(3):229–237. doi:10.1002/zaac.19422490301

[15] Okada S, Iizumi K, Kudaka K, et al. Single crystal growth of (MoXCr1−X)AlB and (MoXW1−X)AlB by metal Al solutions and properties of the crystals. J Solid State Chem. 1997;133(1):36–43. doi:10.1006/jssc.1997.7313

[16] Lu X, Li S, Zhang W, et al. Crack healing behavior of a MAB phase: MoAlB. J Eur Ceram Soc. 2019;39(14):4023–4028. doi:10.1016/j.jeurceramsoc.2019.05.059

[17] Kota S, Zapata-Solvas E, Chen Y, et al. Isothermal and cyclic oxidation of MoAlB in Air from 1100°C to 1400°C. J Electrochem Soc. 2017;164(13):C930–C938. doi:10.1149/2.1891713jes

[18] Xu L, Shi O, Liu C, et al. Synthesis, microstructure and properties of MoAlB ceramics. Ceram Int. 2018;44(11):13396–13401. doi:10.1016/j.ceramint.2018.04.177

[19] Achenbach J-O, Sahu R, Völker B, et al. Synthesis and properties of orthorhombic MoAlB coatings. Coatings. 2019;9(8):510, doi:10.3390/coatings9080510

[20] Evertz S, Pöllmann P, Holzapfel DM, et al. Low temperature synthesis of dense MoAlB thin films. J Eur Ceram Soc. 2021;41(13):6302–6308. doi:10.1016/j.jeurceramsoc.2021.06.046

[21] Yu Y, Lundström T. Crystal growth and structural investigation of the new quaternary compound Mo1−xCrxAlB with x = 0.39. J Alloy Compd. 1995;226(1):5–9. doi:10.1016/0925-8388(95)01598-1

[22] Ade M, Hillebrecht H. Ternary borides Cr_2AlB_2, Cr_3AlB_4, and Cr_4AlB_6: The first members of the series $(CrB_2)nCrAl$ with $n = 1, 2, 3$ and a unifying concept for ternary borides as MAB-phases. Inorg Chem. 2015;54(13):6122–6135. doi:10.1021/acs.inorgchem.5b00049

[23] Hanner LA, Kota S, Barsoum MW. Formation mechanisms of Cr_2AlB_2, Cr_3AlB_4, and Fe_2AlB_2 MAB phases. Mater Res Lett. 2021;9(8):323–328. doi:10.1080/21663831.2021.1912843

[24] Kota S, Wang W, Lu J, et al. Magnetic properties of Cr_2AlB_2, Cr_3AlB_4, and CrB powders. J Alloy Compd. 2018;767:474–482. doi:10.1016/j.jallcom.2018.07.031

[25] Natu V, Kota SS, Barsoum MW. X-ray photoelectron spectroscopy of the MAB phases, MoAlB, M_2AlB_2 (M = Cr, Fe), Cr_3AlB_4 and their binary monoborides. J Eur Ceram Soc. 2020;40(2):305–314.

[26] Bai Y, Qi X, He X, et al. Phase stability and weak metallic bonding within ternary-layered borides CrAlB,

Cr_2AlB_2, Cr_3AlB_4, and Cr_4AlB_6. J Am Ceram Soc. 2019;102(6):3715–3727. doi:10.1111/jace.16206
[27] Khazaei M, Wang J, Estili M, et al. Novel MAB phases and insights into their exfoliation into 2D MBenes. Nanoscale. 2019;11(23):11305–11314. doi:10.1039/C9NR01267B
[28] Rastogi A, Rajpoot P, Verma UP. Study of structural, electronic, optical and thermal properties of refractory material (CrAlB). Mater Chem Phys. 2018;211:242–248. doi:10.1016/j.matchemphys.2018.02.043
[29] Wei J, Zhang L, Liu Y. First-principles calculations study the mechanical and thermal properties of Cr–Al–B ternary borides. Solid State Commun. 2021;326:114182, doi:10.1016/j.ssc.2020.114182
[30] Bogdanovski D, Pöllmann PJ, Schneider JM. An *ab initio* investigation of the temperature-dependent energetic barriers towards CrAlB and (Mo,Cr)AlB formation in a metastable synthesis scenario. Nanoscale. 2022;14(35):12866–12874. doi:10.1039/D2NR01087A
[31] Tang C, Große M, Ulrich S, et al. High-temperature oxidation and hydrothermal corrosion of textured Cr_2AlC-based coatings on zirconium alloy fuel cladding. Surf Coat Technol. 2021;419:127263, doi:10.1016/j.surfcoat.2021.127263
[32] Ström P, Primetzhofer D. Ion beam tools for non-destructive in-situ and in-operando composition analysis and modification of materials at the Tandem Laboratory in Uppsala. Instrum. 2022;17(04):P04011, doi:10.1088/1748-0221/17/04/P04011
[33] Zhang Y, Whitlow HJ, Winzell T, et al. Detection efficiency of time-of-flight energy elastic recoil detection analysis systems. Nucl Instrum Methods Phys Res Sect B. 1999;149(4):477–489.
[34] Ström P, Petersson P, Rubel M, et al. A combined segmented anode gas ionization chamber and time-of-flight detector for heavy ion elastic recoil detection analysis. Rev Sci Instrum. 2016;87(10):103303, doi:10.1063/1.4963709
[35] Janson M. Contes conversion of time-energy spectra a program for ERDA data analysis (internal report, Uppsala university). Internal Report. Uppsala University(Uppsala University); 2004.
[36] Williams DB, Carter CB. Transmission electron microscopy: A textbook for materials science. New York (NY): Springer; 2009.
[37] Michael J, Williams D, Klein C, et al. The measurement and calculation of the X-ray spatial resolution obtained in the analytical electron microscope. J Microsc. 1990;160(1):41–53. doi:10.1111/j.1365-2818.1990.tb03046.x
[38] Kresse G, Furthmüller J. Efficient iterative schemes for *ab initio* total-energy calculations using a plane-wave basis set. Phys Rev B. 1996;54(16):11169–11186. doi:10.1103/PhysRevB.54.11169
[39] Kresse G, Furthmüller J. Efficiency of ab-initio total energy calculations for metals and semiconductors using a plane-wave basis set. Comput Mater Sci. 1996;6(1):15–50. doi:10.1016/0927-0256(96)00008-0
[40] Kresse G, Hafner J. *Ab initio*molecular dynamics for liquid metals. Phys Rev B. 1993;47(1):558–561. doi:10.1103/PhysRevB.47.558
[41] Blöchl PE. Projector augmented-wave method. Phys Rev B. 1994;50(24):17953–17979. doi:10.1103/PhysRevB.50.17953
[42] Kresse G, Joubert D. From ultrasoft pseudopotentials to the projector augmented-wave method. Phys Rev B. 1999;59(3):1758–1775. doi:10.1103/PhysRevB.59.1758
[43] Perdew JP, Burke K, Ernzerhof M. Generalized gradient approximation made simple. Phys Rev Lett 1996;77(18):3865–3868. doi:10.1103/PhysRevLett.77.3865
[44] Monkhorst HJ, Pack JD. Special points for Brillouin-zone integrations. Phys Rev B. 1976;13(12):5188–5192. doi:10.1103/PhysRevB.13.5188
[45] Methfessel M, Paxton AT. High-precision sampling for Brillouin-zone integration in metals. Phys Rev B. 1989;40(6):3616–3621. doi:10.1103/PhysRevB.40.3616
[46] Togo A, Tanaka I. First principles phonon calculations in materials science. Scr Mater. 2015;108:1–5. doi:10.1016/j.scriptamat.2015.07.021
[47] Stoffel RP, Wessel C, Lumey M-W, et al. Ab initio thermochemistry of solid-state materials. Angew Chem, Int Ed. 2010;49(31):5242–5266. doi:10.1002/anie.200906780
[48] Pauling L. Atomic radii and interatomic distances in metals. J Am Chem Soc. 1947;69(3):542–553. doi:10.1021/ja01195a024
[49] Momma K, Izumi F. *VESTA 3* for three-dimensional visualization of crystal, volumetric and morphology data. J Appl Crystallogr. 2011;44(6):1272–1276. doi:10.1107/S0021889811038970
[50] Liu S, Chang K, Mráz S, et al. Modeling of metastable phase formation for sputtered Ti1-xAlxN thin films. Acta Mater. 2019;165:615–625. doi:10.1016/j.actamat.2018.12.004
[51] Liu S, Chang K, Music D, et al. Stress-dependent prediction of metastable phase formation for magnetron-sputtered V1−xAlxN and Ti1−xAlxN thin films. Acta Mater. 2020;196:313–324. doi:10.1016/j.actamat.2020.06.044
[52] Sahu R, Bogdanovski D, Achenbach J-O, et al. Defects in an orthorhombic MoAlB MAB phase thin film grown at moderate synthesis temperature. Nanoscale. 2022;14(7):2578–2585. doi:10.1039/D1NR07792A
[53] Mayrhofer PH, Music D, Schneider JM. Influence of the Al distribution on the structure, elastic properties, and phase stability of supersaturated Ti1−xAlxN. J Appl Phys. 2006;100(9):094906, doi:10.1063/1.2360778
[54] Hogberg H, Hultman L, Emmerlich J, et al. Growth and characterization of MAX-phase thin films [Article. Proceedings Paper]. Surf Coat Technol. 2005;193(1-3):6–10.
[55] Palmquist JP, Li S, Persson POÅ, et al. $M_{n+1}AX_n$ phases in the Ti−Si−C system studied by thin-film synthesis and *ab initio* calculations. Phys Rev B. 2004;70(16):165401, doi:10.1103/PhysRevB.70.165401